Deep origins for the tectal visual processing centers in chordates

Cezar Borba[1], Shea Schwennicke[2], Matthew J. Kourakis[3], William C. Smith[1,3,*]

1. Department of Molecular, Cell and Developmental Biology, University of California, Santa Barbara, CA, USA 93106

2. College of Creative Studies, University of California, Santa Barbara, CA, USA 93106

3. Neuroscience Research Institute, University of California, Santa Barbara, CA, USA 93106

* Corresponding author

Summary

Visuomotor inputs are processed to extract salient features. In vertebrates, the retina projects to processing centers in the midbrain optic tectum (OT; the superior colliculus in mammals) and the lateral geniculate nucleus, with the OT thought to be the more ancient [1]. The advent of the OT in chordates has been clouded by the reported absence of a midbrain homolog in the sister group to the vertebrates, the tunicates [2–7]. The best characterized tunicate nervous system is that of the *Ciona* larva, which, despite having only 177 central nervous system (CNS) neurons, has extensive homology with vertebrates CNSs [8,9]. Here we present anatomical, molecular, behavioral and connectomic data that the larval posterior brain vesicle (pBV) of *Ciona* shares homology with the vertebrate midbrain OT, suggesting their common ancestor possessed a tectum precursor. Moreover, we report that the conservation between the pBV and the OT extends to a role in visual processing. *Ciona* larvae have two distinct visuomotor behaviors - a looming shadow response and negative phototaxis [10]. These are mediated by separate neural pathways that initiate from different clusters of photoreceptors, both projecting to the pBV [11,12]. We report that inputs from both pathways are processed to generate fold-change detection (FCD) outputs [13]. However, the FCD responses differ between the two pathways, with the looming shadow response showing a power relationship to fold-change, while the navigation pathway responds linearly. Significantly, the connectivity and properties of pBV interneurons conform to known FCD circuit motifs, but with different circuit architectures for the two pathways. The negative phototaxis circuit forms an incoherent feedforward loop that involves interconnecting cholinergic and GABAergic interneurons. The looming shadow circuit uses the same cholinergic and GABAergic interneurons, but with different synaptic inputs to create a nonlinear integral feedback loop. These differing circuit architectures are reflected in the differing behavioral outputs.

Results and Discussion

Conserved anatomy, connectivity, and gene expression between the Ciona pBV and vertebrate OT.

The anterior to posterior homologies between the tunicate larval CNS and those of vertebrates have been summarized previously, with the brain vesicle (BV) equated with the vertebrate forebrain, while the *Ciona* motor ganglion (MG), rostral nerve cord, and "neck" show homology to the vertebrate hindbrain, spinal cord, and midbrain/hindbrain junction, respectively (Figure 1A) [8,9]. The *Ciona* BV is further divided into distinct anterior and posterior domains that trace to invariant cell lineages at the 8-cell stage, with the anterior BV (aBV) descending from the a-lineage, and the pBV from the A-lineage (Figure 1A, red and blue cell centroids, respectively) [14–16]. The distribution of neuron types is sharply demarcated by this boundary, with the relay neurons (RN), which make the only descending projections from the BV to the MG, being found exclusively in the pBV [11]. Moreover, the pBV is the primary recipient of projections from the photoreceptors, the gravitactic sensory antennae cells, the coronet cells (putative sensory cells), as well as a subset of peripheral nerves [11,17].

The expression patterns of several genes have led to the hypothesis that tunicates either lack, or have lost, a midbrain, and thus an OT homolog. For example, the gene DMBX, which plays an essential role in vertebrate midbrain development, is not expressed anterior to the MG in *Ciona* [3,4]. In addition, the highly derived tunicate *Oikopleura dioica* (Class Larvacea) does not express the genes *engrailed* or *pax2/5/8* anterior to its hindbrain, suggesting that larvaceans lack a midbrain [6]. Despite the apparent lack of conservation of these genes, a broader reevaluation of published gene expression patterns, as well as new data presented below, show that *Ciona* pBV has a clear midbrain gene expression signature. Most significantly, *Otx*, which is expressed in the developing forebrain and midbrain of vertebrates [18], is expressed in *Ciona* in the developing aBV and pBV [3,19,20], while the *Ciona* ortholog of the vertebrate forebrain maker *dmrt1* [21] is expressed only in the developing aBV [22,23] (Figure 1A). Posterior to the

pBV is the constricted neck region of *Ciona* CNS, which has been equated with the vertebrate MHB, due both to its anatomy and its expression of genes that in vertebrates mark the MHB, such as *pax2/5/8* [3] (Figure 1A). Thus the pBV mirrors the vertebrate midbrain in being bounded by an anterior domain with homology to the forebrain and a posterior domain with MHB homology.

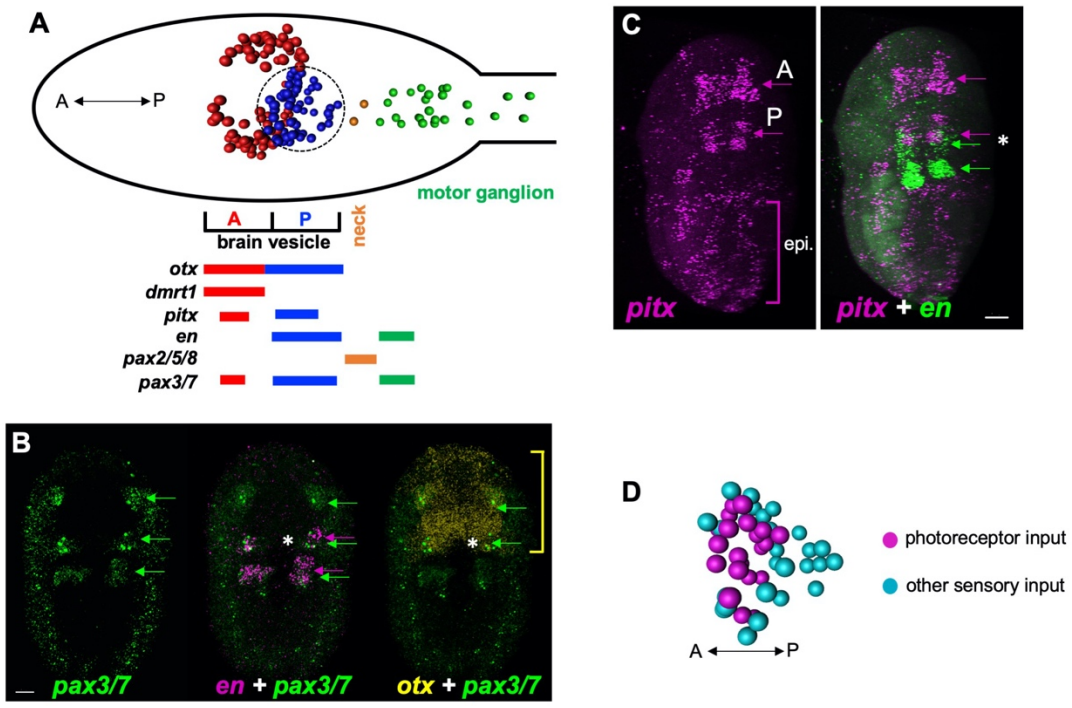

Figure 1. Midbrain homolog in *Ciona*. A. Diagram of the *Ciona* larval CNS with the major brain regions indicated in color. The centroids of neurons are shown, as in Ryan et al., 2016. Below, summary of embryonic gene expression patterns marked by corresponding larval CNS domains. **B.** *In situ* hybridization for *pax3/7*, *en*, and *otx* in early tailbud *Ciona* embryos. The anterior domain of *en*, which marks the presumptive pBV, overlaps with *pax3/7* (asterisk middle panel), and *en* (asterisk right panel). **C.** *In situ* hybridization for *pitx* and *en*. *Pitx* is expressed in anterior and posterior domains in early tailbud embryos. The posterior domain of *pitx* overlaps with the anterior *en* domain in the pBV (asterisk right panel). Diffuse epidermal staining was observed as well. **D.** Spatial distribution of relay neuron types in the pBV corresponds to the circled area in panel A (centroids shown). Abbreviations: A, anterior; P, posterior; epi, epidermis. Anterior is to the left for panel A and D, and to the top for B and C. Scale bars are 10 microns.

The development of the vertebrate optic tectum requires the co-expression of *Pax3*, *Pax7*, *Otx2*, and *En* [24,25]. We observed a similar overlapping expression of *Ciona Pax3/7*,

En, and *Otx2* in the developing *Ciona* pBV at early tailbud stage (Figure 1A and B, asterisk). Additionally, *pitx* has a well-defined role in vertebrate midbrain development [26]. We observed *Ciona pitx* expression at early tailbud stage in the developing pBV that overlaps with *En* expression (Figure 1C, asterisk), as well as in anterior domain that appears to correspond to the aBV expression reported in older embryos and larvae [27]. Finally, the vertebrate optic tectum has a layered morphology with neurons of the superficial layer receiving direct input from the retina, while deeper layers receive and integrate other sensory inputs [28]. The *Ciona* pBV has a layered structure as well, with the RNs receiving photoreceptor input segregated anteriorly, while those receiving input from other sensory systems positioned more posteriorly (Figure 1D). This layering in the pBV of *Ciona* is suggestive of conserved organization between vertebrates and *Ciona*, albeit rudimentary in *Ciona*. Thus, the combination of connectivity, anatomy and gene expression points to the pBV having homology with the vertebrate OT. These results point to a deeper homology for the OT than has previously been appreciated, suggesting an origin predating the divergence of tunicate from vertebrate lineages. The presence of an OT homologous structure in the most basal chordate group, the cephalochordates (including the model Amphioxus), has been the source of speculation and further studies within this group should provide fertile ground toward the ultimate resolution of the appearance and modification of this structure over time [5,29].

Fold-change detection in Ciona.

Light-driven behaviors in *Ciona* initiate at the ocellus, a photosensitive organ in the BV that consists of three lens cells, a single pigment cell, and 30 ciliary photoreceptors in two distinct clusters, named the PR-I and PR-II groups [11,30]. The PR-I and PR-II pathways split visual input into two components, with the PR-I pathway providing information on the direction of light - and thereby mediating phototaxis, while the PR-II pathway responds to changes in ambient light [10,12]. In fact, both pathways respond to illumination changes, as the PR-I

associated pigment cell cup selectively, and directionally, shades the photoreceptors as the larvae perform casting swims, allowing them to discern the direction of light. Many biological systems that respond to temporally changing stimuli transform inputs to make the system responsive to relative fold-change, rather than to absolute stimulus levels [13]. A fundamental property of fold-change detection (FCD) is that increases in the fold-change of a stimulus give an increased output. To investigate *Ciona* photoresponses, 25-hour post-fertilization larvae were exposed to a fold-change dimming series using a 505 nm LED lamp while recording at far-red (700 nm), as described previously [12,31]. The series ranged from 3-fold (600 lux to 200 lux) to 60-fold (600 lux to 10 lux) dimming, Figure 2A and Figure S1. Several parameters were measured in the dimming-induced swims: percent of larvae responding to dim, and the swim time, velocity, and tortuosity of responding larvae. Video S1 shows representative responses to 3-, 10- and 60-fold dims. Of these parameters, induced swim time showed a positive relation to increased fold-change (Figure 2A), while velocity and tortuosity were constant across the series (Figure 2B and Figure S1). The percent of larvae responding to dimming increased initially with fold change, but plateaued at around 10-fold, and thus did not appear to be a manifestation of FCD behavior (Figure S1). While the dimming response is an output of the PR-II pathway, we reported previously that in larvae homozygous for the pigmentation mutant *pristine* the PR-I photoreceptors can be experimentally assessed using ambient light changes because they are no longer shielded by pigment [10]. Since there are more PR-I photoreceptors than PR-II (30 versus 7), it is likely that the PR-I output predominates in *pristine* larvae. In fact, we find that *pristine* larvae are more sensitive to dimming at low-light conditions than wild type (Figure S2). Thus with the *pristine* mutant we can assess the response of the PR-I pathway to fold-change input. When the same fold-change dimming series was performed on *pristine* larvae we again observed a positive relationship of swim time to fold-change, but with a significantly different response curve (Figure 2C and Figure S1), suggesting a different circuit at play [32]. The best fit curve for wild-type swim times versus fold-change was a power slope having an $R^2 = 0.98$.

While the log slope of this curve also had an $R^2 = 0.98$, the Bayesian information criterion (BIC, see Methods) for a power relationship had the lower score, indicating a better fit (-13 and 17 for power and log, respectively; $R^2 = 0.87$ for linear). The best fitting model for the *pristine* swim times is a linear slope having an $R^2 = 1.00$ ($R^2 = 0.92$ and 0.81 for power and log, respectively).

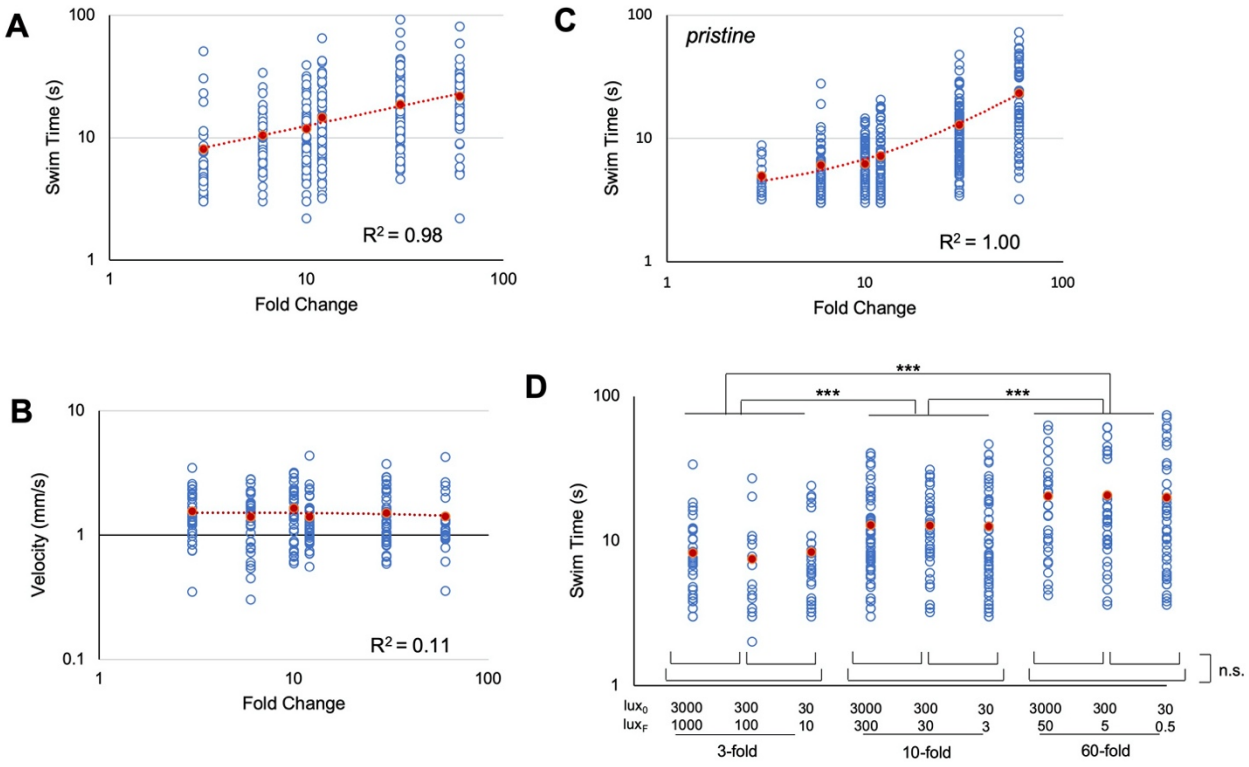

Figure 2. Fold-change detection in *Ciona* photoresponses. **A.** Larval swim times in response to different fold-change light dimming (3-fold to 60-fold) increase as a power function (log/log plot shown). All data points (blue circles) and averages (red circles) are shown. **B.** Swim velocity is constant across fold-change dimming series. **C.** Larval swim times of homozygous *pristine* mutants in response to different fold-change light dimming. **D**. Dimming at same fold-change but different absolute values across three orders of magnitude gives the same swim times. Lux_0, initial illumination level in lux; Lux_F, illumination after dim, in lux. ***, $p<0.01$; n.s., not significant. See **Figures S1** and S**3** for full data presentation, including sample sizes, average values, and statistical analyses.

One of the defining properties of FCD is that stimuli of the same fold-change, but of different absolute magnitudes, will give the same output [13]. We find this holds true for the *Ciona* dimming response across three orders of magnitude. For example, while we observed a significant increase in average swim time between 3-, 10- and 60-fold dims, the swim times

between 10-fold dims of 3000 to 300 lux, 300 to 30 lux, and 30 to 3 lux were not different, likewise with 3- and 60-fold dims (Figure 2D and Figure S3). Another property of FCD systems is exact adaptation, meaning that the system returns to the baseline state even when the modulated stimulus persists at the new state [33]. This behavior was observed in *Ciona* larvae responding to a dimming stimulus (Video S2). In the video, larvae are initially at 3000 lux, which is then dimmed to 300 lux. The majority of the larvae swim in response to the dim but return to being stationary after approximately 30 seconds. The majority of the larvae then remain stationary until a second dim two minutes later to 30 lux again evokes swimming. A final predicted property of FCD systems is that the reaction time should decrease as fold change increases [13], which we observed as a power-slope increase in reaction time as the fold-change decreased (Figure S4).

The utility of FCD transformation of visual input for *Ciona* larvae is evident. In negative phototaxis, a larva discerns the direction of light by casting swims, and it is the decrease in illumination falling on the PR-Is as the larva turns away from the light that is the cue to swim. If larvae were responding only to absolute light levels, the amount of light falling on the PR-Is when facing away from a bright source versus facing towards a dim source could have the same values. Adaptation alone, which would extend the range of light intensities detected, would not give a consistent behavioral output in changing ambient light conditions. The utility of FCD to the dimming response is similar. If only absolute light intensities were controlling swim behavior, the same looming object that appeared to be a threat in one ambient light condition, might not in another.

Visual processing circuitry in the Ciona pBV

The simplicity of the *Ciona* CNS means that there are few candidate cells and circuits for performing the FCD transformation. The ocellus alone is unlikely to be able to give an FCD output. While photoreceptor adaptation likely contributes to the illumination ranges across which

Ciona shows FCD behavior (Figure 2D), adaptation alone does not give fold-change detection [33]. In addition, tunicate photoreceptors, like their vertebrate counterparts, are hyperpolarizing and, most importantly, have graded outputs [34,35]. Finally, the *Ciona* ocellus lacks the complex interneuron architecture of the vertebrate retina, rather the photoreceptors project directly to the pBV. The MG, likewise, does not appear to be a good candidate to contain the FCD circuits. Is it dominated by excitatory cholinergic interneurons and motor neurons, while inhibitory neurons, which would be an essential modulatory element of any likely FCD circuit, are limited to the GABAergic AMG neurons, which received no descending input, directly or indirectly, from the photoreceptors or BV, and the glycinergic decussating ACINs, which likely play a role in the central pattern generator, not visual processing [11,12,36]. Instead, the pBV because of its complex interconnections of inhibitory and excitatory RNs [12], and proposed homology to the vertebrate OT, is a much better candidate to possess the FCD circuits (Figure 3A). In fact, the recent description of visual and gravitaxis sensory integration by pBV RNs already demonstrates a sensory processing function for the pBV [31].

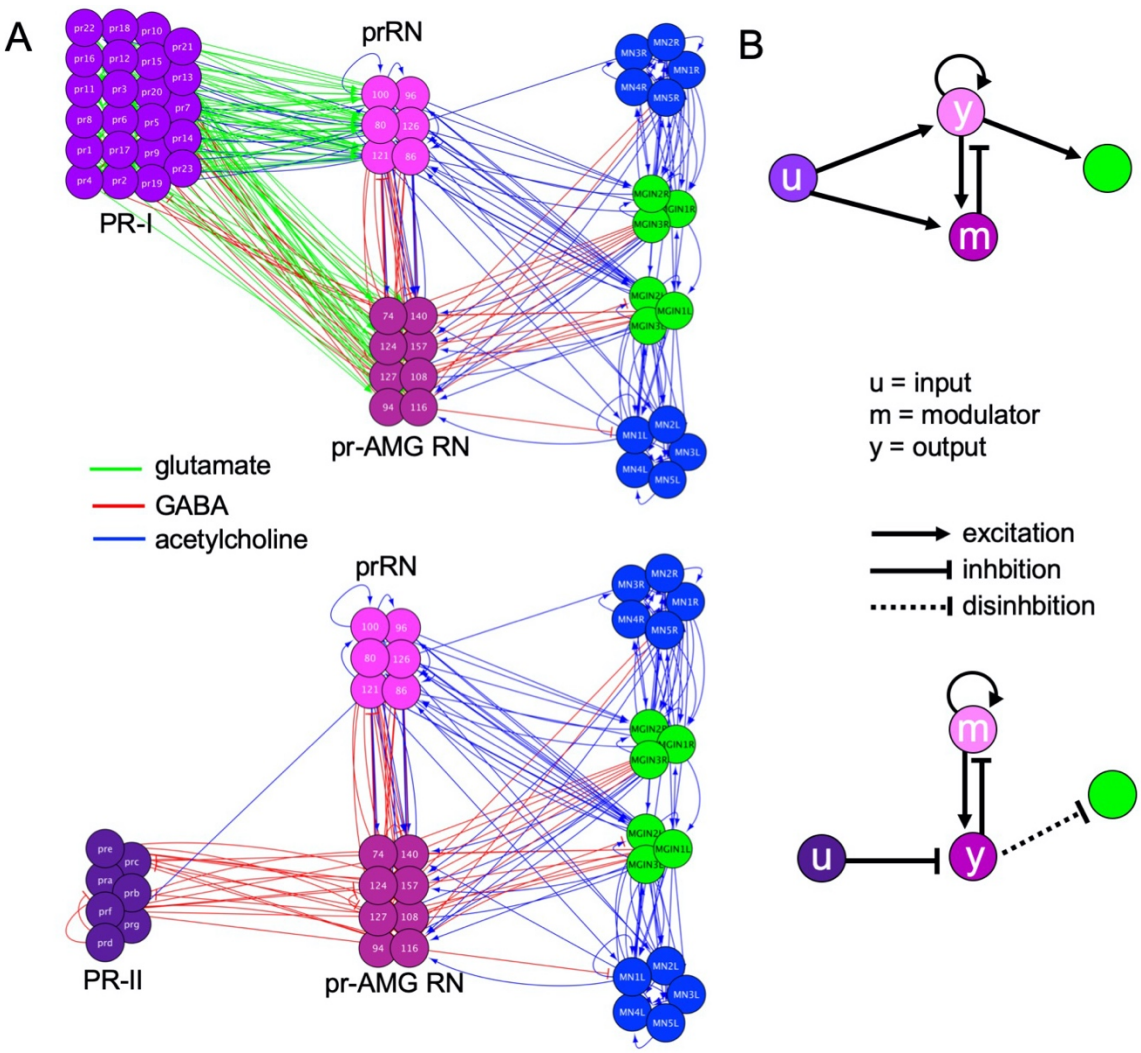

Figure 3. Photoresponse pathways and putative fold-change detection circuits. **A.** Full circuits for the PR-I (top) and PR-II (bottom) pathways from the *Ciona* connectome (Ryan et al., 2016). Neurotransmitter use for synaptic connections (lines) is based on Kourakis et al., 2019. Abbreviations: PR, photoreceptor; prRN, photoreceptor relay neuron, pr-AMG RN, photoreceptor ascending motor ganglion relay neurons; MGIN motor ganglion interneurons; MN motor neurons. **B**. Simplified circuits for the PR-I (top) and PR-II (bottom) pathways derived by combining like cells and assigning valence of synapses (excitatory or inhibitory) based on consensus for that cell type. Nodes are labeled according to proposed function (*i.e.*, input modulator, and output). Colors of nodes and neurons are according to cell-types in [11].

The ocellus photoreceptors project directly to two distinct types of RNs in the pBV (Figure 3A). The six *photoreceptor RN*s (prRN) receive input exclusively from the glutamatergic PR-Is. *In situ* hybridization and pharmacological studies indicate the prRNs are primarily cholinergic [12]. The second cluster of eight RNs, the *photoreceptor ascending motor ganglion*

*RN*s (pr-AMG RN), are mostly (or perhaps exclusively) GABAergic [12], and are postsynaptic to both the PR-I and GABAergic PR-II photoreceptors [11]. There are also extensive synaptic connections between the pr-AMG RNs and the prRNs within the pBV. The PR-I and PR-II pathways then converge on a common set of cholinergic interneurons and motor neurons in the MG (the MGINs and MNs, respectively; Figure 3A). While the PR-I pathway projects excitatory input to the MG via the prRNs, the PR-II pathway is more complex, and a combination of neurotransmitter use, pharmacological and mutant analyses strongly indicates that this pathway activates the MG via disinhibition [12,31]. When we simplify the PR-I and PR-II circuits by combining cell types and synaptic connections we see the emergence of two likely FCD circuits (Figure 3B). The PR-I circuit (top, Figure 3B) appears to make an incoherent feedforward loop (IFFL) [13]. This IFFL is more complex than the widely studied Type-1 IFFL, which contains only three elements, but computer modeling of an IFFL circuit similar to the one proposed here was predicted to give an FCD output (circuit 04040 [37]). The PR-II circuit, being disinhibitory, is more unusual, but strongly resembles a nonlinear integral feedback loop (NLIFL), but with the modulator (m) being excitatory rather than inhibitory (bottom, Figure 3B). Note that in the two FCD circuits in Figure 3B that the RN types exchange roles as output and modulator, suggesting an economy of neuron use.

To experimentally support the proposed FCD neural circuits, the modulator component of the PR-II dimming circuit was manipulated pharmacologically. In the proposed PR-II circuit, the modulators are the cholinergic prRNs (Figure 3B). Previous work showed coexpression of glutamatergic AMPA receptors with VACHT in pBV neurons, but not on GABAergic pBV neurons [12]. The AMPA receptors on the prRNs are targets of the glutamatergic PR-Is, as the AMPA receptor antagonist perampanel inhibits phototaxis, but not the dimming response [12]. Therefore, to selectively modulate the cholinergic prRNs while not disrupting the PR-II output, larvae were treated with AMPA (500μM), an agonist of AMPA receptors. This treatment should result in tonic depolarization of the modulatory prRNs. When assessed in the fold-change

dimming series, the percentage of AMPA-treated larvae responding was no different than controls (Video S3). However, the behavioral response curve in the fold-change series was significantly shallower in the AMPA-treated sample in comparison to controls (Figure 4 and Figure S5). In other words, while the larvae still respond to dimming they appear to have a greatly reduced FCD response. Moreover, these results also support the FCD circuit residing in the pBV, as the photoreceptors lack AMPA receptors (Figure S6).

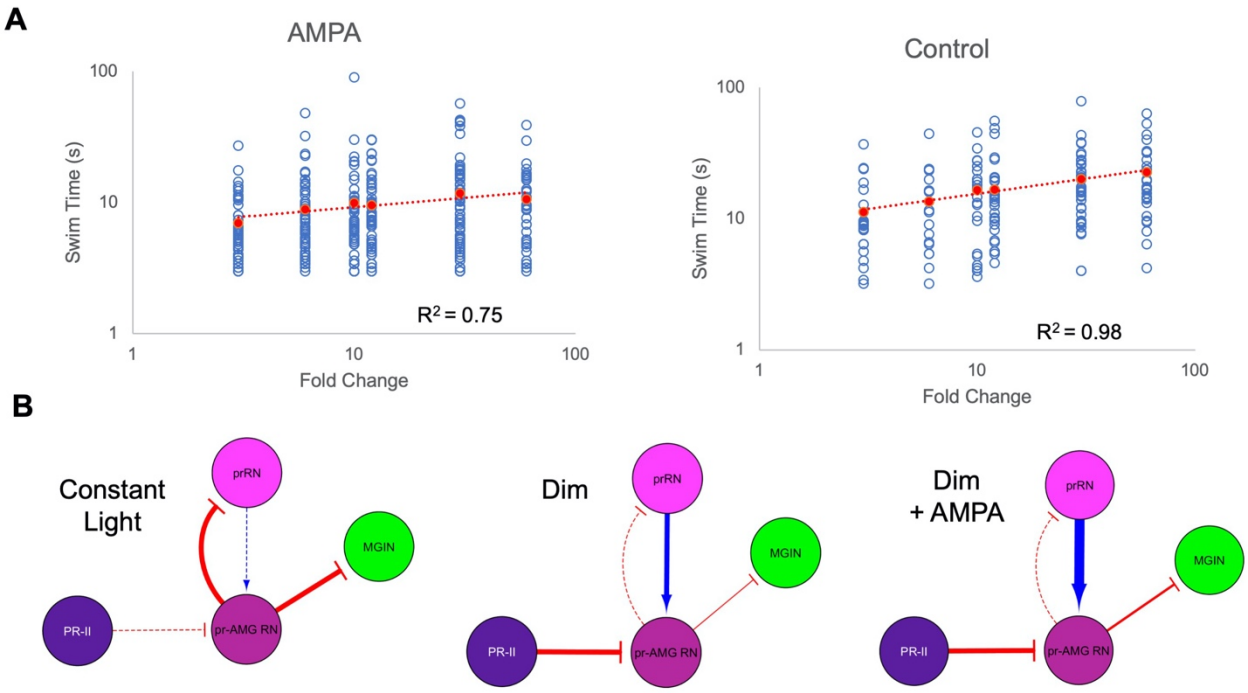

Figure 4. Disruption of PR-II FCD circuit by AMPA. A. Swim times of control and AMPA-treated larvae in a fold-change dimming series. All data points (blue circles) and averages (red circles) are shown. The swim times for the AMPA-treated larvae do not show the same increase with increased fold-change as do the controls. **B**. Model of AMPA disruption of the PR-II FCD circuit. AMPA gives a tonic depolarization of the modulatory prRNs resulting in greater excition of the output inhibitory pr-AMG RNs. See **Figures S6** for full data presentation, including sample sizes, average values, and statistical analyses.

Figure 4B shows a model of the manipulation. In constant light (left panel), the inhibitory pr-AMG RNs are constitutively active, a prediction of the disinhibition model [12]. In control larvae, dimming results in inhibition of the pr-AMG RNs by the GABAergic PR-IIs, which in turn reduces inhibition of the cholinergic prRNs, setting up the modulator of the FCD circuit (middle

panel). With AMPA present during the dim, the prRNs are tonically depolarized, disrupting their modulatory role in the FCD circuit and resulting in little change between steps in the fold-changes series (right panel). These results are consistent with the proposed FCD circuit architecture for the PR-II pathway. At present we know of no similar pharmacological test of the PR-I FCD circuit.

In summary, the *Ciona* pBV processes sensory inputs to direct simple behaviors, such as the dimming response and body orientation with respect to external stimuli (*i.e.*, light and gravity). By contrast, vertebrate sensory inputs and behaviors are much more complex than those observed in *Ciona* larvae, and the OT and other CNS processing regions of vertebrates extract much greater depth of spatial and temporal information from sensory inputs [1,28,38]. Accordingly, the OT of even the most primitive vertebrates contains orders of magnitude more neurons than the *Ciona* pBV, which is composed of only several dozen neurons. Nevertheless, the vertebrate OT also mediates simple orientation and escape behaviors, similar to those observed in *Ciona* [1,39,40]. Thus, the similarities highlighted here between the *Ciona* pBV and the vertebrate OT suggests that these may be ancestral functions of a conserved brain region.

References

1. Knudsen, E.I. (2020). Evolution of neural processing for visual perception in vertebrates. J. Comp. Neurol. *epub*. https://onlinelibrary.wiley.com/doi/abs/10.1002/cne.24871 \.
2. Striedter, G., and Northcutt, R.G. (2020). Brains Through Time: A Natural History of Vertebrates (Oxford University Press).
3. Ikuta, T., and Saiga, H. (2007). Dynamic change in the expression of developmental genes in the ascidian central nervous system: revisit to the tripartite model and the origin of the midbrain-hindbrain boundary region. Dev. Biol. *312*, 631–43.
4. Takahashi, T., and Holland, P.W.H. (2004). Amphioxus and ascidian Dmbx homeobox genes give clues to the vertebrate origins of midbrain development. Development *131*, 3285–3294.
5. Lacalli, T.C. (2006). Prospective protochordate homologs of vertebrate midbrain and MHB, with some thoughts on MHB origins. Int. J. Biol. Sci., 104–109.
6. Cañestro, C., Bassham, S., and Postlethwait, J. (2005). Development of the central nervous system in the larvacean Oikopleura dioica and the evolution of the chordate brain. Dev. Biol. *285*, 298–315.
7. Holland, L.Z. (2017). 1.01 - Invertebrate Origins of Vertebrate Nervous Systems. In Evolution of Nervous Systems (Second Edition), J. H. Kaas, ed. (Oxford: Academic Press),

pp. 3–23.
8. Hudson, C. (2016). The central nervous system of ascidian larvae. Wiley Interdiscip Rev Dev Biol.
9. Wada, H., Saiga, H., Satoh, N., and Holland, P.W. (1998). Tripartite organization of the ancestral chordate brain and the antiquity of placodes: insights from ascidian Pax-2/5/8, Hox and Otx genes. Development *125*, 1113–22.
10. Salas, P., Vinaithirthan, V., Newman-Smith, E., Kourakis, M.J., and Smith, W.C. (2018). Photoreceptor specialization and the visuomotor repertoire of the primitive chordate Ciona. J Exp Biol *221*.
11. Ryan, K., Lu, Z., and Meinertzhagen, I.A. (2016). The CNS connectome of a tadpole larva of Ciona intestinalis (L.) highlights sidedness in the brain of a chordate sibling. Elife *5*. e16962
12. Kourakis, M.J., Borba, C., Zhang, A., Newman-Smith, E., Salas, P., Manjunath, B., and Smith, W.C. Parallel visual circuitry in a basal chordate. Elife 26. e44753
13. Adler, M., and Alon, U. (2018). Fold-change detection in biological systems. Curr. Opin. Syst. Biol. *8*, 81–89.
14. Nicol, D., and Meinertzhagen, I.A. (1988). Development of the central nervous system of the larva of the ascidian, Ciona intestinalis L. I. The early lineages of the neural plate. Dev. Biol. *130*, 721–36.
15. Nicol, D., and Meinertzhagen, I.A. (1988). Development of the central nervous system of the larva of the ascidian, Ciona intestinalis L. II. Neural plate morphogenesis and cell lineages during neurulation. Dev. Biol. *130*, 737–66.
16. Nishida, H., and Satoh, N. (1983). Cell lineage analysis in ascidian embryos by intracellular injection of a tracer enzyme. I. Up to the eight-cell stage. Dev Biol *99*, 382–94.
17. Ryan, K., Lu, Z., and Meinertzhagen, I.A. (2018). The peripheral nervous system of the ascidian tadpole larva: Types of neurons and their synaptic networks. J Comp Neurol *526*, 583–608.
18. Boyl, P.P., Signore, M., Annino, A., Barbera, J.P.M., Acampora, D., and Simeone, A. (2001). Otx genes in the development and evolution of the vertebrate brain. Int. J. Dev. Neurosci. *19*, 353–363.
19. Imai, K.S., Satoh, N., and Satou, Y. (2002). Region specific gene expressions in the central nervous system of the ascidian embryo. Mech Dev *119 Suppl 1*, S275-7.
20. Hudson, C., Darras, S., Caillol, D., Yasuo, H., and Lemaire, P. (2003). A conserved role for the MEK signalling pathway in neural tissue specification and posteriorisation in the invertebrate chordate, the ascidian Ciona intestinalis. Development *130*, 147–159.
21. Kikkawa, T., Obayashi, T., Takahashi, M., Fukuzaki-Dohi, U., Numayama-Tsuruta, K., and Osumi, N. (2013). Dmrta1 regulates proneural gene expression downstream of Pax6 in the mammalian telencephalon. Genes Cells *18*, 636–649.
22. Tresser, J., Chiba, S., Veeman, M., El-Nachef, D., Newman-Smith, E., Horie, T., Tsuda, M., and Smith, W.C. (2010). doublesex/mab3 related-1 (dmrt1) is essential for development of anterior neural plate derivatives in Ciona. Development *137*, 2197–203.
23. Wagner, E., and Levine, M. (2012). FGF signaling establishes the anterior border of the Ciona neural tube. Development *139*, 2351–2359.
24. Matsunaga, E., Araki, I., and Nakamura, H. Role of Pax3/7 in tectum development. 9.
25. Thompson, J.A., Zembrzycki, A., Mansouri, A., and Ziman, M. (2008). Pax7 is requisite for maintenance of a subpopulation of superior collicular neurons and shows a diverging expression pattern to Pax3 during superior collicular development. BMC Dev. Biol. *8*, 62.
26. Luk, K.C., Rymar, V.V., Munckhof, P. van den, Nicolau, S., Steriade, C., Bifsha, P., Drouin, J., and Sadikot, A.F. (2013). The transcription factor Pitx3 is expressed selectively in midbrain dopaminergic neurons susceptible to neurodegenerative stress. J. Neurochem. *125*, 932–943.
27. Christiaen, L., Burighel, P., Smith, W.C., Vernier, P., Bourrat, F., and Joly, J.-S. (2002). Pitx

genes in Tunicates provide new molecular insight into the evolutionary origin of pituitary. Gene *287*, 107–113.
28. Cang, J., Savier, E., Barchini, J., and Liu, X. (2018). Visual Function, Organization, and Development of the Mouse Superior Colliculus. Annu. Rev. Vis. Sci. *4*, 239–262.
29. Lacalli, T. (2018). Amphioxus, motion detection, and the evolutionary origin of the vertebrate retinotectal map. EvoDevo *9*, 6.
30. Horie, T., Sakurai, D., Ohtsuki, H., Terakita, A., Shichida, Y., Usukura, J., Kusakabe, T., and Tsuda, M. (2008). Pigmented and nonpigmented ocelli in the brain vesicle of the ascidian larva. J Comp Neurol *509*, 88–102.
31. Bostwick, M., Smith, E.L., Borba, C., Newman-Smith, E., Guleria, I., Kourakis, M.J., and Smith, W.C. (2020). Antagonistic Inhibitory Circuits Integrate Visual and Gravitactic Behaviors. Curr. Biol., 30, 600-609.
32. Adler, M., Mayo, A., and Alon, U. (2014). Logarithmic and power law input-output relations in sensory systems with fold-change detection. PLoS Comput Biol *10*, e1003781.
33. Shoval, O., Goentoro, L., Hart, Y., Mayo, A., Sontag, E., and Alon, U. (2010). Fold-change detection and scalar symmetry of sensory input fields. Proc Natl Acad Sci U A *107*, 15995–6000.
34. McReynolds, J.S., and Gorman, A.L.F. (1975). Hyperpolarizing photoreceptors in the eye of a primitive chordate, Salpa democratica. Vision Res. *15*, 1181–1186.
35. Gorman, A.L., McReynolds, J.S., and Barnes, S.N. (1971). Photoreceptors in primitive chordates: fine structure, hyperpolarizing receptor potentials, and evolution. Science *172*, 1052–4.
36. Nishino, A., Okamura, Y., Piscopo, S., and Brown, E.R. (2010). A glycine receptor is involved in the organization of swimming movements in an invertebrate chordate. BMC Neurosci *11*, 6.
37. Adler, M., Szekely, P., Mayo, A., and Alon, U. (2017). Optimal Regulatory Circuit Topologies for Fold-Change Detection. Cell Syst. *4*, 171-181.e8.
38. Basso, M.A., and May, P.J. (2017). Circuits for Action and Cognition: A View from the Superior Colliculus. Annu. Rev. Vis. Sci. *3*, 197–226.
39. Dunn, T.W., Gebhardt, C., Naumann, E.A., Riegler, C., Ahrens, M.B., Engert, F., and Del Bene, F. (2016). Neural Circuits Underlying Visually Evoked Escapes in Larval Zebrafish. Neuron *89*, 613–28.
40. Shang, C., Chen, Z., Liu, A., Li, Y., Zhang, J., Qu, B., Yan, F., Zhang, Y., Liu, W., Liu, Z., *et al.* (2018). Divergent midbrain circuits orchestrate escape and freezing responses to looming stimuli in mice. Nat. Commun. *9*, 1232.
41. Veeman, M.T., Chiba, S., and Smith, W.C. (2011). Ciona genetics. Methods Mol Biol *770*, 401–22.
42. Yoshida, K., and Saiga, H. (2008). Left–right asymmetric expression of Pitx is regulated by the asymmetric Nodal signaling through an intronic enhancer in Ciona intestinalis. Dev. Genes Evol. *218*, 353–360.
43. Newman-Smith, E., Kourakis, M.J., Reeves, W., Veeman, M., and Smith, W.C. (2015). Reciprocal and dynamic polarization of planar cell polarity core components and myosin. Elife *4*.
44. Horie, T., Orii, H., and Nakagawa, M. (2005). Structure of ocellus photoreceptors in the ascidian Ciona intestinalis larva as revealed by an anti-arrestin antibody. J Neurobiol *65*, 241–50.

STAR Methods

Animals.

Wild type *Ciona robusta* (a.k.a., *Ciona intestinalis* type A) were collected from the Santa Barbara Yacht harbor. The animals carrying the mutation *pristine* [10] were cultured at the UC Santa Barbara Marine Lab[41]. Larvae were obtained by mixing dissected gametes of 3 adults and then culturing in natural seawater at 18°C. Homozygous *prs* larvae were produced by natural spawning of heterozygous or homozygous *prs* adults.

Hybridization chain reaction (HCR) in situ and immunostaining.

Whole mount *in situ* hybridization of embryonic or larval *C. robusta* were performed as previously described [12]. Briefly, fluorescent labeling was achieved following the hybridization chain reaction (v. 3.0) of Molecular Instruments (Los Angeles). Complementary RNA probe sets were designed to coding regions for the following *C. robusta* genes: *Otx*, *en*, *pax3/7*, *AMPA receptor*, and *pitx*. In larvae which underwent both *in situ* labeling and immunostaining, the *in situ* hybridization was performed first, followed by the immunolabeling (see below), after a transition from 5X SSCT to PBST. Larvae for immunostaining were dechorionated at mid-tailbud stage using sodium thioglycolate, as for *in situ* hybridization, so that left-right asymmetric properties of the CNS would not be disrupted [42]. The immunostaining followed previously described procedures for *Ciona* [43]. A primary antibody against *C. robusta* arrestin [44], raised in rabbit, was used at a dilution of 1:1000. A secondary antibody, α-rabbit AlexaFluor 594 (Invitrogen), was also used at 1:1000. Labeled animals (either by *in situ* or immunohistochemistry) were imaged on an Olympus Fluoview 1000 confocal microscope; post-image analysis used Imaris v5.0 or ImarisViewer v9.5.1 as well as Fiji (ImageJ) v. 2.0.0-rc-69/1.52p.

Behavioral Assays.

All larvae were between 25 and 28 hours post fertilization (hpf) (18^{o}C). Larval swimming behaviors were recorded in sea water with 0.1% BSA using agarose-coated petri dishes to reduce sticking. Image series were collected using a Hamamatsu Orca-ER camera fitted on a Navitar 7000 macro zoom lens. Programmable 700 nm and 505 nm LED lamps (Mightex) mounted above the petri dishes were used for dimming response assays as previously described [12]. The dim response, adaptation, and reaction time videos were recorded at 5, 8.9, and 50 frames per second (fps), respectively. In the standard assay larvae were recorded for 10s at the initial intensity (lux_0) that was then dimmed (lux_F) to specific values while image capture continued for 2 min. Larvae were allowed to recover for 5 min before being assayed again. All light intensity readings were taken with an Extech Instruments light meter.

Drug Treatments.

(*RS*)-AMPA hydrobromide (Tocris) was dissolved in filtered sea water to a stock concentration of 7.5 mM and then diluted to a final concentration of 500 µM. Larvae were incubated with the drug for about 10 min before beginning assays.

Behavioral Quantification.

Larvae with short bouts of swimming (<3s) were not scored [12,31]. Swim times, velocities, and tortuosities were calculated using the MATLAB script ELIANE [12] and the larvae scored between the conditions were tested for significance using the Wilcoxon Rank-Sum test. Percent of larvae that responded were quantified manually and tested for significance using the Student T-Test. R-squared values and Bayesian information criterion (BIC) were calculated using the program R. Larvae that had stuck to the petri dish, or that swam to the edges or into other larvae were not scored.

Acknowledgments

The work was supported by an award from the NIH (NS103774) to W.C.S, and a CCS Create Fund Summer Fellowship to S.S.. We thank Takehiro Kusakabe for the anti-Arrestin antibody.

Author contributions.

C.B. and M. J. K. contributed to experimental design, data collection and analysis, and manuscript preparation. S.S. contributed to data collection and analysis. W.C.S. contributed to research funding, experimental design, data collection and analysis, and manuscript preparation.

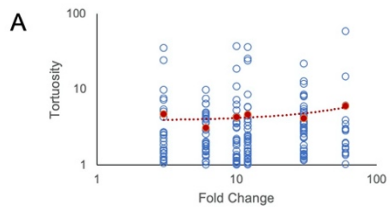

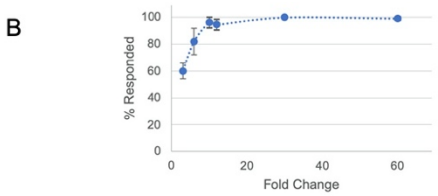

C

Experimental *n*-values

Fold Change	WT Swim Time	PRS Swim Time	Velocity	Tortuosity	% Respond
3	38	15	29	29	127
6	44	56	36	36	102
10	53	70	35	35	105
12	68	72	36	36	125
30	79	90	41	41	132
60	48	56	20	20	143

D

Experiment Averages ± Standard Deviation

Fold Change	WT Swim Time	PRS Swim Time	Velocity	Tortuosity	% Respond
3	8.07±9.15	4.97±1.82	1.56±0.99	4.75±14.69	60.06±5.95
6	10.45±6.30	6.07±4.22	1.40±0.98	3.12±14.27	81.94±9.89
10	11.88±7.95	6.24±2.78	1.65±0.96	4.30±13.85	96.16±4.01
12	14.63±11.38	7.19±4.40	1.41±0.94	4.70±13.48	94.61±4.06
30	18.70±14.80	12.84±8.26	1.51±0.92	4.14±13.15	100.00±0.00
60	21.86±13.98	23.30±15.99	1.42±0.90	6.07±12.82	99.19±1.41

E

Statistical Test *p*-values

WT Swim Times

FC	3	6	10	12	30
6	4.29E-04				
10	2.79E-04	0.2665			
12	1.41E-05	0.0223	0.1093		
30	1.34E-07	1.78E-05	2.67E-04	0.0088	
60	1.77E-07	2.17E-07	2.56E-06	1.18E-04	0.0194

PRS Swim Times

FC	3	6	10	12	30
6	0.2721				
10	0.035	0.0565			
12	0.0464	0.0446	0.3559		
30	1.09E-06	7.99E-12	1.74E-11	1.12E-08	
60	5.89E-08	1.46E-14	8.21E-16	1.04E-13	5.85E-06

Velocity

FC	3	6	10	12	30
6	0.4095				
10	0.8292	0.2206			
12	0.2222	0.7740	0.2385		
30	0.5197	0.7323	0.5048	0.6867	
60	0.1895	0.7517	0.2446	0.5901	0.4024

Tortuosity

FC	3	6	10	12	30
6	0.7665				
10	0.6563	0.5011			
12	0.7365	0.5849	0.9587		
30	0.2379	0.4717	0.1595	0.1269	
60	0.5085	0.9932	0.6058	0.5668	0.6727

% Respond

FC	3	6	10	12	30
6	0.0304				
10	0.0010	0.0823			
12	0.0011	0.1096	0.6618		
30	0.0003	0.0342	0.1729	0.0832	
60	0.0004	0.0404	0.2854	0.1390	0.3739

Fold-Change	WT vs. PRS
3	0.6642
6	2.05E-06
10	9.94E-07
12	5.14E-08
30	0.0018
60	0.8962

Figure S1. Expanded data for fold-change assays. **A**. Swim tortuosity [10] plotted as a function of fold-change dimming. **B**. Percent of larvae responding in fold-change dimming series. **C.** Number of larvae analyzed in plots of swim time [wild type (WT) and *pristine*], velocity, percent responding and tortuosity versus fold-change dimming. **D**. Experimental averages in plots swim time [wild type (WT) and *pristine*], velocity and tortuosity versus fold-change dimming. **E**. Pairwise tests for significance at each fold-change for swim time [wild type (WT) and *pristine*], velocity, percent responding and tortuosity (P-values shown; all comparisons by Wilcoxon, except percent responding which was done by T-test). Also shown is a comparison of swim times in WT and pristine (PRS) larvae at each fold-change step. P-values for each comparison are listed. FC = fold change.

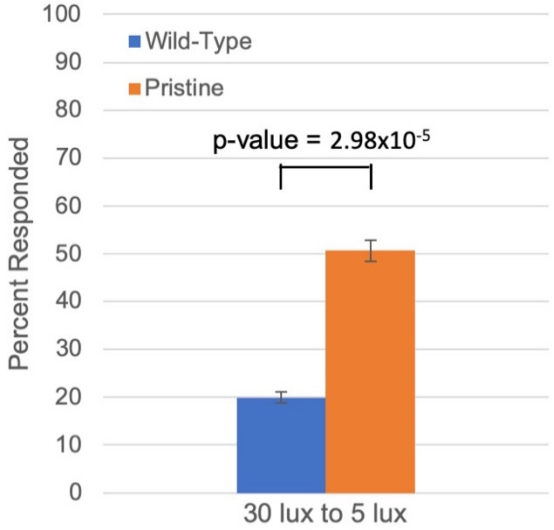

Figure S2. Percent of larvae responding to six-fold dim at low illumination conditions (30 lux to 5 lux). *n*= 76 and 131, for wild-type and pristine, respectively. P value from T-test.

A

Experiment Data

Fold Change	3-fold			10-fold			60-fold		
Δlux	3000to1000	300to100	30to10	3000to300	300to30	30to3	3000to50	300to5	30to0.5
Average ± SD	8.23±5.89	7.49±6.42	8.35±5.74	12.81±9.41	12.74±7.95	12.56±10.90	20.32±15.43	20.61±16.86	19.92±19.55
n	39	19	34	62	39	54	31	34	43

B

Statistical Test p-values

within fold changes

3-fold	3000to1000	300to100
300to100	0.7327	
30to10	0.3187	0.4726

10-fold	3000to300	300to30
300to30	0.7246	
30to3	0.2942	0.2705

60-fold	3000to50	300to5
300to5	0.2737	
30to0.5	0.8595	0.3729

between fold changes

	3-fold	10-fold
10-fold	1.88E-05	
60-fold	4.36E-11	2.79E-04

Figure S3. Expanded data for fold-change assay). A. Average swim times, standard deviations, and number of larvae analyzed for data presented in Figure 2D. **B. Left.** Comparisons of swim times in assays with same fold-change, but different absolute illumination values each fold-change. **Right.** Comparisons of pooled swim times at 3-, 10-, and 60-fold dimming. All tests of significance by Wilcoxon. P values shown. FC = fold change.

A

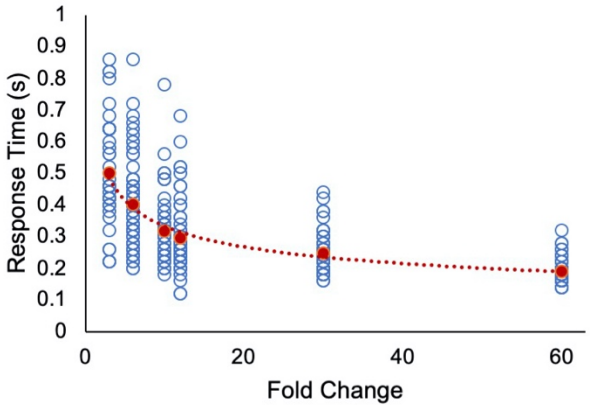

B

Experiment Data

Fold-Change	Average ± SD	n
3	0.50±0.17	39
6	0.40±0.14	65
10	0.32±0.10	64
12	0.30±0.11	55
30	0.25±0.06	52
60	0.19±0.04	49

C

Statistical Test p-values

FC	3	6	10	12	30
6	3.80E-03				
10	2.56E-08	1.65E-04			
12	2.45E-08	5.39E-06	0.0701		
30	5.14E-12	2.51E-11	7.00E-06	0.009	
60	1.03E-14	1.91E-17	5.01E-15	2.30E-10	2.28E-07

Figure S4. Reaction time as a function of fold-change. **A.** Plot of the reaction time versus fold change. All data points (blue circles) and averages (red circles) are shown. **B.** Expanded data for graph. **C.** Statistical test of significance (Wilcoxon).

A

Experiment values

	AMPA		Control	
Fold Change	Swim Time	n	Swim Time	n
3	6.97±4.58	47	11.24±8.24	22
6	8.86±7.77	57	13.55±10.29	17
10	9.96±12.82	51	16.44±11	22
12	9.56±7.15	57	16.6±12.69	31
30	11.79±10.63	72	20.04±13.75	37
60	10.58±7.68	36	22.59±13.77	30

B

Statistical Test (p-values)

AMPA

FC	3	6	10	12	30
6	0.1340				
10	0.0680	0.3932			
12	0.0332	0.2563	0.3343		
30	0.0023	0.0343	0.0620	0.1397	
60	0.0089	0.0801	0.1145	0.1971	0.5570

Control

FC	3	6	10	12	30
6	0.3100				
10	0.0422	0.1977			
12	0.0216	0.1883	0.5144		
30	5.11E-04	0.0181	0.1775	0.0561	
60	1.36E-04	0.0051	0.0515	0.0122	0.1737

AMPA vs Control	
3-fold	0.0074
6-fold	0.0257
10-fold	4.30E-03
12-fold	5.40E-04
30-fold	2.54E-05
60-fold	1.46E-05

Figure S5. Expanded data for AMPA-treated larvae. A. Average swim times and sample sizes for APMA-treated and control larvae. **B.** Left and middle tables compare swim times between fold-changes in APMA-treated and control larvae, the right table compares swim times at each fold-change between AMPA-treated and control larvae. P-values are shown (Wilcoxon). FC = fold change.

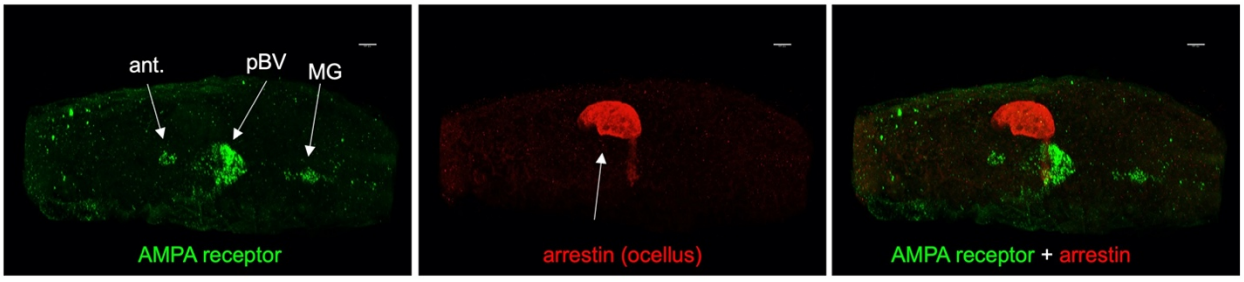

Figure S6. AMPA receptor is not expressed in the ocellus. AMPA receptor detected by *in situ* hybridization (green), while the ocellus photoreceptor marker Arrestin was detected by immunostaining (red).

Video S1. Response of *Ciona* larvae to 3-, 10- and 60-fold dimming. Video plays at 5X normal speed.

Video S2. Absolute adaptation. Larvae are exposed to two dimming events separated by 2 minutes. The first dim is from 3000 to 300 lux, and the second from 300 lux to 30. Video plays at 5X normal speed.

Video S3. Response of APMA-treated and control larvae to a 60-fold dim. Video plays at 5X normal speed.